ISSN 0036-0236, Russian Journal of Inorganic Chemistry, 2013, Vol. 58, No. 6, pp. 695–700. © Pleiades Publishing, Ltd., 2013.
Original Russian Text © Z.A. Mikhailovskaya, E.S. Buyanova, S.A. Petrova, M.V. Morozova, R.G. Zakharov, V.M. Zhukovskii, 2013, published in Zhurnal Neorganicheskoi Khimii, 2013, Vol. 58, No. 6, pp. 787–792.

PHYSICAL METHODS OF INVESTIGATION

Structure and Electrical Conductivity of Cobalt-Doped $Bi_{26}Mo_{10}O_{69}$

Z. A. Mikhailovskaya[a], E. S. Buyanova[a], S. A. Petrova[b], M. V. Morozova[a], R. G. Zakharov[b], and V. M. Zhukovskii[a]

[a] *Ural Federal University Named after the First Russian President El'tsin, Yekaterinburg, Russia*
[b] *Institute of Metallurgy, Ural Branch, Russian Academy of Sciences, Yekaterinburg, Russia*

Received November 15, 2011

Abstract—The existence boundaries, structures, and transport parameters of $Bi_{1-x}Co_x[Bi_{12}O_{14}]Mo_5O_{20\pm\delta}$ and $Bi[Bi_{12}O_{14}]Mo_{5-y}Co_yO_{20\pm\delta}$ solid solutions, which have a unique columnar structure, were studied. Electrical conductivity in these solid solutions was studied by impedance spectroscopy.

DOI: 10.1134/S003602361306017X

Many complex oxides of the Bi_2O_3–MoO_3 system have bright catalytic properties and are therefore well studied [1–5]. In particular, they are highly selective catalysts for oxidation and oxidative ammonolysis of olefins [6–9]. Bismuth molybdate of 1 : 1 composition (Bi_2MoO_6 exists in three polymorphs [10]. The low-temperature Bi_2MoO_6 phase (γ(L), koechlinite) is an Aurivillius phase, which consists of an alternation of $(Bi_2O_2)_n$ layers and a layer formed by disordered MoO_6 octahedra [11]. When heated in the region of 840 K, the γ(L) phase reversibly transforms to a transient medium-temperature γ''(I) phase, which is also an orthorhombic Aurivillius phase where an oxygen–molybdenum layer is formed of MoO_4 tetrahedra [12]. Lastly at 877 K an irreversible transition occurs from γ''(I) to a high-temperature γ'(H) phase. The structure of γ'(H)-Bi_2MoO_6 was established by high-resolution X-ray powder diffraction [13] and single-crystal X-ray diffraction [14]: cations form a fluorite-like network, which consists of infinite channels composed of Bi–O polyhedra and surrounded by MoO_4 tetrahedra.

A high-bismuth region of the Bi_2O_3–MoO_3 system is studied insufficiently; in particular, there are controversial data on the extent of solid solutions based on the $Bi_{26}Mo_{10}O_{69\pm\delta}$ phase [15, 16]. The structure of $Bi_{26}Mo_{10}O_{69\pm\delta}$ ($Bi_{13}Mo_5O_{34\pm\delta}$), which has been established comparatively recently, is close to the structure of stoichiometric $Bi(Bi_{12}O_{14})Mo_4VO_{20\pm\delta}$ [17] and is related to the structure of γ'(H)–Bi_2MoO_6. This structure can be described as a network of infinite columns (channels) $(Bi_{12}O_{14})_n$, surrounded by $(Mo,V)O_4$ polyhedra and additional isolated bismuth atoms. This complex oxide and its base substitutional solid solutions ($Bi_{26}Mo_{10-x}M_xO_{69\pm\delta}$ and $Bi_{26-x}M_xMo_{10}O_{69\pm\delta}$, where M = Ca, Sr, Ba, Pb, or W) [18] are promising one-dimensional oxygen-ion conductors.

Here, we study the substitutions of cobalt atoms for bismuth and molybdenum positions in $Bi_{26}Mo_{10}O_{69\pm\delta}$. These substitutions are theoretically possible, as follows from a comparison of the ionic radii of bismuth(+3) and cobalt(+2) in a coordination surrounding with CN = 8 ($r_{Bi^{3+}} = 1.17$ Å, $r_{Co^{2+}} = 0.9$ Å; substitution at the position of an isolated bismuth atom) and a comparison of the radii of cobalt(+2) and molybdenum(+6) in a tetrahedral surrounding ($r_{Co^{2+}} = 0.58$ Å, $r_{Mo^{6+}} = 0.41$ Å, substitution of cobalt for molybdenum positions in an MoO_4 tetrahedron) [19].

EXPERIMENTAL

The subject matters of this study were solid solutions samples: $Bi_{1-x}Co_x[Bi_{12}O_{14}]Mo_5O_{20\pm\delta}$, where $x = 0.2–1$, with $\Delta x = 0.2$; and $Bi[Bi_{12}O_{14}]Mo_{5-y}Co_yO_{20\pm\delta}$, where $y = 0.2, 0.4$. Complex oxide powders were prepared by standard ceramic technology in the temperature range 770–1170 K in 100-K steps with 10-h exposure at each step. The compositions of the initial mixtures, intermediates, and final products were monitored using X-ray powder diffraction (D8 ADVANCE diffractometer, CuK_α radiation, β filter, position-sensitive VÅNTEC detector). Unit cell parameters were calculated and the structure was refined using TOPAS [20] and FullProf [21] program packages. Particle sizes were determined on a SALD-7101 Shimadzu dispersion analyzer. Densitometric analysis involved pycnometric density measurements using isopropanol as working liquid. Differential thermal analysis was performed in the temperature range 290–1070 K using an STA 409 PC Luxx Netzsch thermal analyzer. The reference used was alumina. Samples for conductivity measurements were powders of the test phases compacted into briquettes 10 mm in diameter and sintered at 1170 K (the final synthesis temperature) for 24 h. Microstructures of sintered samples were examined using JEOL JSM 6390LA scanning electron microscope equipped with a JED 2300 X-ray energy-dispersive microanalyzer. Electrical conductivity was studied

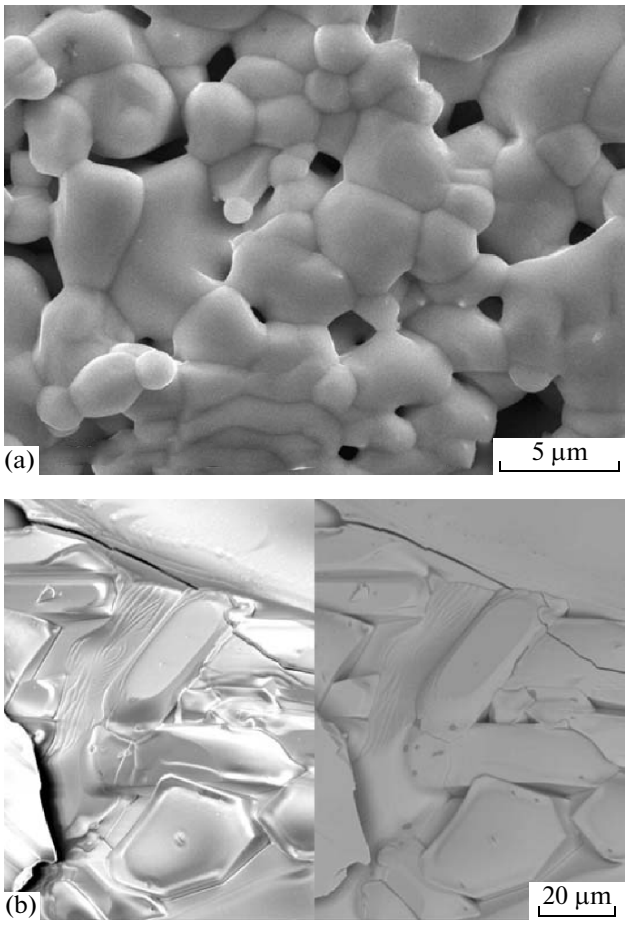

Fig. 1. Secondary and back-scattered electron images of (a) surface and (b) cleave of a $Bi_{12.8}Co_{0.2}Mo_5O_{34\pm\delta}$ briquette at various magnifications.

using impedance spectroscopy (Elins Z-2000 and Elins Z-3000 impedance meters) in the range 1070–470 K.

RESULTS AND DISCUSSION

Synthesis and Structure

In designing an experiment to prepare solid solutions, we took into account that in order for the bismuth sublattice of bismuth molybdate $Bi_{26}Mo_{10}O_{69}$ to be doped, the substituent atom should acquire a coordination surrounding with CN = 8, and in order for the molybdenum sublattice to be doped, it should have CN = 4. According to [19], neither of these surrounding types is intrinsic to a cobalt ion with the oxidation number +3; its preferred coordination is with CN = 6. Therefore, the cobalt oxidation number in these compounds was formally taken to be +2, for the reason that both cubic and tetragonal oxygen coordinations are intrinsic to Co^{2+} ions. Unfortunately, the determination of an actual cobalt oxidation number was strongly hampered by small cobalt concentrations (1.1 at % without oxygen atoms and 0.4 at % with oxygen atoms taken into account).

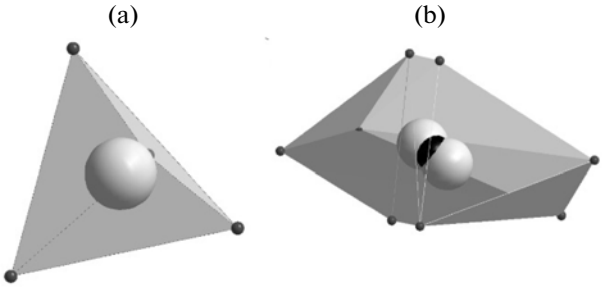

Fig. 2. Coordination surrounding of the Mo(1) atom: (a) in the parent bismuth molybdate $Bi_{13}Mo_5O_{34\pm\delta}$ and (b) doped $Bi_{12.8}Co_{0.2}Mo_5O_{34\pm\delta}$. Large balls: molybdenum atoms; small balls: oxygen atoms.

X-ray powder diffraction showed that the solid solution of composition $Bi_{1-x}Co_x[Bi_{12}O_{14}]Mo_5O_{20\pm\delta}$ was formed only when $x = 0.2$, as proven by electron microscopy. Figure 1 displays secondary and back-scattered electron images of the surface and cleave of a sintered $Bi_{12.8}Co_{0.2}Mo_5O_{34\pm\delta}$ sample at various magnifications. One can see that this sample is homogeneous; the intergrain region is pure. At higher dopant concentrations, a second phase appears, which is isostructural to γ-Bi_2MoO_6 (orthorhombic space group *Pca*21, a = 5.5019(2) Å, b = 16.2449(7) Å, c = 5.5237(1) Å). When $x = 1$, the sample has an X-ray diffraction patent fully identical to this compound;

Table 1. Phase composition and density of $Bi_{1-x}Co_x[Bi_{12}O_{14}][MoO_4]_{5\pm\delta}$ solid solutions

As-batch composition	Phase composition	ρ_{calc}, g/cm^3	ρ_{obs}, g/cm^3
$Bi_{12.8}Co_{0.2}Mo_5O_{34\pm\delta}$	$Bi_{12.8}Co_{0.2}Mo_5O_{34\pm\delta}$	7.51	7.46
$Bi_{13}Mo_5O_{34\pm\delta}$	97% $Bi_{12.8}Co_{0.2}Mo_5O_{34}$ + 3% $Bi_{12}CoMo_5O_{34\pm\delta}$	7.53	7.57
$Bi_{13}Mo_5O_{34\pm\delta}$	90% $Bi_{12.8}Co_{0.2}Mo_5O_{34}$ + 10% $Bi_{12}CoMo_5O_{34\pm\delta}$	7.57	7.67
$Bi_{13}Mo_5O_{34\pm\delta}$	65% $Bi_{12.8}Co_{0.2}Mo_5O_{34}$ + 35% $Bi_{12}CoMo_5O_{34\pm\delta}$	7.72	7.85
$Bi_{13}Mo_5O_{34\pm\delta}$	$Bi_{13}Mo_5O_{34\pm\delta}$	8.11	8.00

therefore, the formula $Bi_{12}CoMo_5O_{34 \pm \delta}$ can be assigned to a sample of as-batch composition $Bi_2Mo_{5/6}Co_{1/6}O_{6 \pm \delta}$ (by analogy with Bi_2MoO_6).

A tentative theoretical density of a sample having an intermediate composition was calculated as a linear combination of the densities of two phases, as follows:

$$\rho_{\text{phase mixture}} = \rho_{\text{phase1}}\omega_{\text{phase1}} + \rho_{\text{phase2}}\omega_{\text{phase2}}, \quad (1)$$

where $\rho_{\text{phase mixture}}$, ρ_{phase1}, and ρ_{phase2} are, respectively, the sought density and the densities of the constituent phases of the mixture; ω_{phase1} and ω_{phase2} are, respectively the weight fractions of the phases.

The theoretical density of a single-phase sample was taken to be the X-ray density. The results are displayed in Table 1. Nice agreement is observed between the theoretically calculated and experimentally determined compositions and relations of phases. The results of energy-dispersive X-ray microanalysis for $Bi_{12.8}Co_{0.2}Mo_5O_{34 \pm \delta}$ show somewhat inhomogeneous distribution of cobalt atoms over the bulk of the sample; the average cobalt content, however, is close to the as-batch composition and agrees with the results of elemental analysis ($\omega_{Co}^{theor} = 1.11$, $\omega_{Co}^{AES} = 1.06$, $\omega_{Co}^{SEM} = 1.52$ at %).

Noteworthy, the closeness of bismuth and molybdenum lines in the energy-dispersive spectrum cannot provide a reliable determination of each of these elements, but allows their overall content to be determined quite exactly. When cobalt is doped into the molybdenum sublattice, solid solution formation is also limited to $y = 0.2$. As the dopant concentration increases, bismuth molybdate of composition $Bi_{38}Mo_7O_{78}$ is segregated. The resulting powders have particle sizes within a range of 1–10 μm.

$PbBi_{12}Mo_5O_{34}$ and $Bi_{13}Mo_5O_{34 \pm \delta}$ were chosen to be the initial structures in the refinement of crystal structure for single-phase samples [15, 22]. The thermal factors of light (oxygen) atoms in both cases were not refined because of a strong disorder intrinsic to the oxygen sublattices in these compounds. No substantial changes in coordinates relative to the initial compound have been found. Table 2 displays exemplary results of calculations for $Bi_{12.8}Co_{0.2}Mo_5O_{34 \pm \delta}$. Compared to undoped $Bi_{13}Mo_5O_{34 \pm \delta}$ (a = 11.742(0) Å, b = 5.800(0) Å, c = 24.770(0) Å, β = 102.(94)° [21]) $Bi_{12.8}Co_{0.2}Mo_5O_{34 \pm \delta}$ (a = 11.723(44) Å, b = 5.796(38) Å, c = 24.697(88) Å, β = 102.(08)°) has decreased values of the parameter a and angle β in a unit cell; the same was noticed for $PbBi_{12}Mo_5O_{34}$. This can arise either from the smaller radius of an isolated atom in the structure, or from the absence of the $6s^2$ lone pair in a cobalt atom, which endows bismuth with donor–acceptor interactions with columnar structure fragments. The results of calculations for $Bi_{13}Mo_{4.8}Co_{0.2}O_{34 \pm \delta}$ (a = 11.716(29) Å, b = 5.792(04) Å, c = 24.738(56) Å, β = 102.(68)°) show increased values of c and β compared to $Bi_{12.8}Co_{0.2}Mo_5O_{34 \pm \delta}$. These increased values can be due to not only the incorporation of cobalt atoms into the molybdenum sublattice but also to the formation in this case of $[BiO_3E]$ polyhedra, where E stands for the $6s^2$ lone pair of bismuth; the formation of this pair is also suggested in [17, 23].

Table 2. Structure parameters of $Bi_{12.8}Co_{0.2}Mo_5O_{34 \pm \delta}$ (space group P_12/c, a = 11.723(44) Å, b = 5.796(38) Å, c = 24.697(88) Å, β = 102.08°)

Atom	x	y	z	Occupancy	B_{iso}
Bi(1)	0.0405	0.4134	0.3270	0.98	0.42
Bi(2)	0.1616	–0.0870	0.2469	0.95	0.55
Bi(3)	0.2412	0.0034	0.3992	0.95	0.54
Bi(4)	0.3592	0.4889	0.3233	0.94	0.53
Bi(5)	0.2708	0.4983	0.1598	0.98	0.60
Bi(6)	0.0822	–0.0053	0.0915	0.94	0.42
Bi(7)	0.5180	0.4604	0.0080	0.38	3.14
Co	0.5180	0.4604	0.0080	0.22	3.14
Mo(1)	0.4893	0.0213	0.2391	0.53	0.62
Mo(2)	0.1690	0.5152	0.4866	0.96	0.92
Mo(3)	0.4237	0.0032	0.0783	1.02	0.63
O(1)	0.000	0.257	0.250	0.99	1.00
O(2)	0.000	–0.268	0.250	1.02	1.00
O(3)	0.252	0.269	0.337	0.48	1.00
O(4)	0.280	0.816	0.357	1.01	1.00
O(5)	0.185	0.842	0.238	1.01	1.00
O(6)	0.147	0.931	0.071	0.69	1.00
O(7)	0.161	0.237	0.154	1.02	1.00
O(8)	0.055	0.131	0.372	0.94	1.00
O(9)	0.380	0.208	0.221	0.25	1.00
O(10)	0.382	0.199	0.242	0.75	1.00
O(11)	0.532	–0.001	0.146	0.97	1.00
O(12)	0.464	–0.211	0.171	0.49	1.00
O(13)	0.387	0.120	0.008	1.02	1.00
O(14)	0.243	–0.139	0.100	1.01	1.00
O(15)	0.465	–0.311	0.082	1.01	1.00
O(16)	0.456	0.215	0.066	0.99	1.00
O(17)	0.233	0.621	0.568	1.04	1.00
O(18)	0.287	0.426	0.453	1.01	1.00
O(19)	0.107	0.749	0.483	1.01	1.00
O(20)	0.071	0.246	0.443	0.94	1.00

Note: $R_{Bragg} = 1.96$, $R_F = 2.64$, and $R_p = 6.03$.

As follows from the structure refinement, the molybdenum position Mo1 is split in both of the aforementioned compounds. The atom Mo1 is in tight contact with two $[Bi_{12}O_{14}]_n$ columns and has a complex double tetrahedral surrounding. This is illustrated by Fig. 2, which images the coordination surrounding in

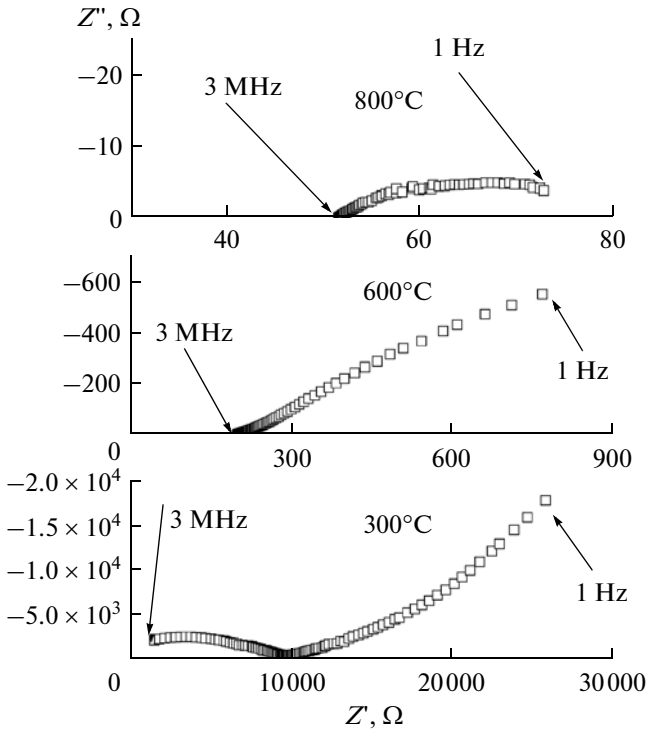

Fig. 3. Representative impedance curves for $Bi_{13}Mo_{4.8}Co_{0.2}O_{34\pm\delta}$ at various temperatures.

doped and undoped $Bi_{13}Mo_5O_{34\pm\delta}$, where real molybdenum and oxygen coordinates in the crystal structure are used. Small changes in the configuration of columns and in distances between them can influence the molybdenum position. For example, comparing site occupancies in the initial structure and in the structure of a $Bi_{12.8}Co_{0.2}Mo_5O_{34\pm\delta}$, one can see a small decrease in site occupancy for bismuth atoms in $[Bi_{12}O_{14}]_n$ columns, but for isolated atoms, site occupancies remain at the previous level and are well fitted by a combination of site occupancies for the cobalt and bismuth atoms that reside in this position. The high thermal factor intrinsic to these atoms is due to the split of their position into a pair of closely lying positions with random distribution over them. This effect is observed both in the host compound and in all cobalt-doped samples. When different oxidation numbers for cobalt are introduced into calculations, the general structure pattern remains unchanged.

In order to evaluate the thermal stability of test samples, high-temperature thermal studies were carried out. Neither weight change nor thermal events are observed in the temperature range 300–1120 K, and this proves the nonoccurrence of phase transitions or decomposition of complex oxides in air over the range of temperatures studied.

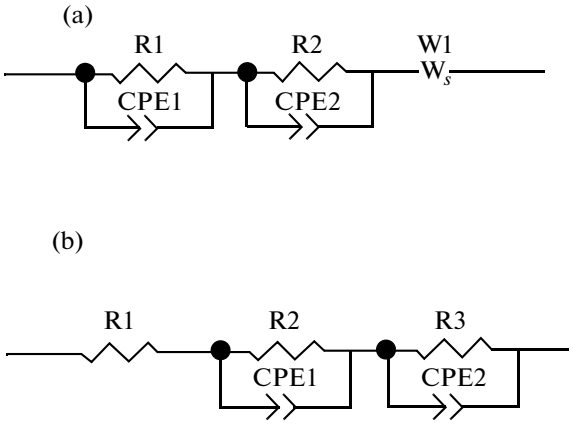

Fig. 4. Equivalent circuits that fit impedance curves: (a) low temperatures and (b) high temperatures.

Electrical Conductivity

Two-probe impedance spectroscopy using platinum electrodes in the cooling mode was used to study the electrical conductivity of solid solutions. Measurements were carried out both for single-phase and multiphase samples. Figure 3 shows representative impedance spectra for $Bi_{13}Mo_{4.8}Co_{0.2}O_{34\pm\delta}$ at different temperatures. This type of spectrum is characteristic of all test samples. The equivalent circuit of the cell that corresponds to the occurrence of processes in a certain temperature range was selected using Zview software (Version 2.6b, Scribner Associates, Inc.). One can see that the dependence of the imaginary part of the complex impedance on the real part changes in response to changing temperature. At relatively low temperatures,

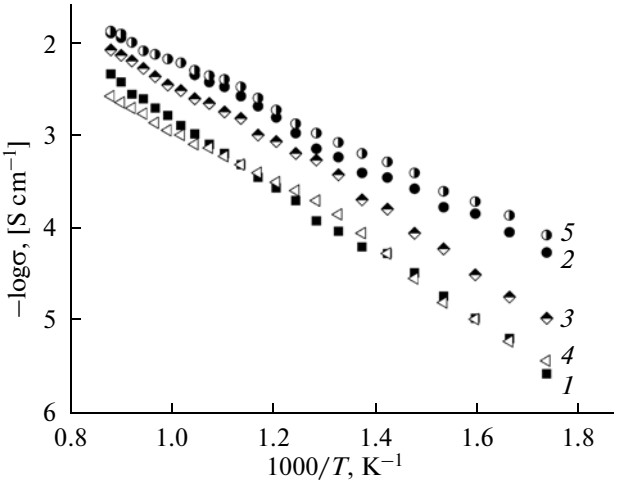

Fig. 5. Electrical conductivity versus temperature for solid solutions $Bi_{1-x}Co_x[Bi_{12}O_{14}]Mo_5O_{20\pm\delta}$, where (*1*) $x = 0$, (*2*) $x = 0.2$, (*3*) $x = 0.8$, and (*4*) $x = 1$, and for $Bi[Bi_{12}O_{14}]Mo_{5-y}Co_yO_{20\pm\delta}$ solid solutions, where (*5*) $y = 0.2$.

Table 3. Comparison of electrochemical parameters of the studied and known electrolytes

Composition	$-\log\sigma_{700}$ [S cm^{-1}]	$-\log\sigma_{350}$ [S cm^{-1}]	E_a, eV
$Bi_{0.8}Co_{0.2}[Bi_{12}O_{14}]Mo_5O_{20\pm\delta}$	2.24	3.87	0.52
$Bi[Bi_{12}O_{14}]Mo_{4.8}Co_{0.2}O_{20\pm\delta}$	2.23	3.74	0.51
$Ce_{0.8}Gd_{0.2}O_{1.9}$ [25]	~1.9	~5	1.03
YSZ [26]	~1–2	~3.5–4.5	~0.9–1.05

the curve features an asymmetric semicircle. Further, the impedance curve smoothly transforms to a straight line with a slope close to 45°. Thus, the cell circuit for the low-temperature range is a series connection of resistors R1 and R2 with parallel-connected CPE1 and CPE2, which characterize the electrolyte material, and a closed Warburg diffusion element W1 (Fig. 4a). CPE elements in the equivalent circuit denote constant-phase elements.

The resistor R1 and CPE1 in parallel connection correspond to the bulk conductivity of a sample; R2 and CPE2 correspond to the grain-boundary resistance of grains, and their sum corresponds to overall resistance. Thus, the conductivity of a polycrystalline sample at low temperatures was calculated proceeding from the value of R1 + R2. The Warburg element W_s describes the occurrence of diffusion processes in the chosen temperature range. The orders of magnitude of capacitance of CPE2 and CPE1 (10^{-8} and 10^{-11} F) allow them to be assigned to grain-boundary and bulk conductivity, respectively [24]. Increasing temperature considerably enhances oxygen diffusion and adsorption on electrodes, and the Warburg element leaves the circuit (Fig. 4b). The impedance curve now looks as a semicircle of a smaller radius, which transforms to a semicircle of a larger radius. The small semicircle (connection of R2 and CPE2) may be assigned to the grain-boundary resistance, while the semicircle corresponding to the bulk resistance is leveled out and characterized only by the value of resistor R1. As at low temperatures, the overall resistance will be characterized by the sum of R1 and R2. The parallel connection of R3 and CPE3 in this case describes those electrode processes in the measured system that are undetectable at low temperatures on the background of diffusion processes. The capacitance of CPE2 is on the order of 10^{-8} F and that of CPE3 is 10^{-6} F, which is typical of oxide systems.

The measurements showed a considerable increase in electrical conductivity relative to the host compound. Figure 5 displays concentration- and temperature-dependent electrical conductivity curves. For cobalt doping, in the sample doped with cobalt in the molybdenum sublattice, the electrical conductivity was found to be slightly higher than in the sample doped with the same cobalt amount in the bismuth sublattice. Most likely, doping into the molybdenum sublattice is more efficient due to the transfer of isolated bismuth atoms to the molybdenum sublattice and the formation of BiO_3E tetrahedra. Castro et al. [23] suggest that the $6s^2$ lone pair of an discrete bismuth atom inhibits oxygen diffusion, and removal of bismuth from the discrete position would increase the electrical conductivity. The compound with $x = 1$, which is isostructural to Bi_2MoO_6, showed lower values. Table 3 compares the values of activation energies and electrical conductivities for the newly studied and known materials. Judging from the values found in the range 670–770 K, these materials are competitive with known oxygen-ion conductors and can be tested as electrolytes for electrochemical devices.

ACKNOWLEDGMENTS

This study was supported by the Russian Foundation for Basic Research (project nos. 12-03-00464 and 12-03-31119) and the Federal Target Program "Research and Research Training Resources of Innovative Russia" (Governmental Contract nos. 14.132.21.1455 and 14.132.21.1470).

REFERENCES

1. L. Ya. Erman, E. L. Gal'perin, and B. P. Sobolev, Zh. Neorg. Khim. **6** (2), 490 (1971).
2. S. Miyazawa, A. Kawana, and H. Koizumi, Mater. Res. Bull. **9**, 41 (1974).
3. T. Chen and S. Smith, J. Solid State Chem. **13** (4), 288 (1975).
4. D. J. Buttrey, D. A. Jeferson, and J. M. Thomas, Mater. Res. Bull. **21** (6), 739 (1985).
5. L. E. Depero and L. Sangaleti, J. Solid State Chem. **119** (2), 428 (1995).
6. R. K. Grasselli, Appl. Catal. **15** (1), 127 (1985).
7. J. D. Burrington, C. T. Kartisek, and R. K. Grasselli, J. Catal. **87** (2), 363 (1984).
8. D. J. Hucknall, *Selective Oxidation of Hydrocarbons* (Academic Press, New York, 1974).
9. T. Uda, T. T. Lin, and G. W. Keulks, J. Catal. **62** (1), 26 (1980).

10. H. Kodama and A. Watanabe, J. Solid State Chem. **56** (2), 225 (1985).
11. K. S. Knight, Mineral. Mag. **56**, 399 (1992).
12. V. I. Voronkova, E. P. Kharitonova, and O. G. Rudnitskaya, J. Alloys Compd. **487** (1–2), 274 (2009).
13. D. J. Buttrey, T. Vogt, U. Wildgruber, and W. R. Robinson, J. Solid State Chem. **111**, 118 (1994).
14. P. Begue, R. Enjalbert, J. Galy, et al., Solid State Sci. **2**, 637 (2000).
15. R. N. Vannier, G. Mairesse, F. Abraham, et al., J. Solid State Chem. **122**, 394 (1996).
16. D. J. Buttrey, T. Vogt, G. P. A. Yap, et al., Mater. Res. Bull. **32**, 947 (1997).
17. R. Enjalbert, G. Hassselmann, and J. Galy, J. Solid State Chem. **131**, 236 (1997).
18. R. N. Vannier, S. Danze, G. Nowogrocki, et al., Solid State Ionics **136–137**, 51 (2000).
19. R. D. Shannon, Acta Crystallogr. **32**, 751 (1976).
20. Diffrac Plus (Bruker, Karlsruhe, 2006).
21. J. Rodriguez-Carvajal, Physica B **192** (1–2), 55 (1993).
22. R. Enjalbert, G. Hasselmann, and J. Galy, Acta Crystallogr. C **53**, 269 (1997).
23. A. Castro, R. Enjalbert, P. Baules, and J. Galy, J. Solid State Chem. **139**, 185 (1998).
24. J. T. S. Irvine, D. C. Sinclair, and A. R. West, Adv. Mater. **2** (3), 132 (1990).
25. E. Yu. Pikalova, A. A. Murashkina, V. I. Maragou, et al., Inter. J. Hydrogen Energy **36** (10), 6175 (2011).
26. J. H. Joo and G. M. Choi, Solid State Ionics **177**, 1053 (2006).

Translated by O. Fedorova